Journal Pre-proof

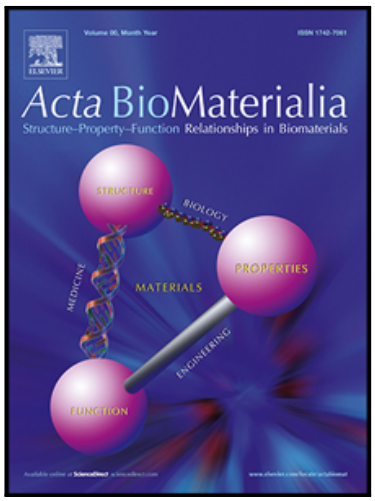

Preparation of Cetyl Palmitate-based PEGylated Solid Lipid Nanoparticles by Microfluidic technique

Ilaria Arduino , Zehua Liu , Antti Rahikkala , Patrícia Figueiredo , Alexandra Correia , Annalisa Cutrignelli , Nunzio Denora , Hélder A. Santos

PII: S1742-7061(20)30738-8
DOI: https://doi.org/10.1016/j.actbio.2020.12.024
Reference: ACTBIO 7092

To appear in: *Acta Biomaterialia*

Received date: 24 September 2020
Revised date: 9 December 2020
Accepted date: 10 December 2020

Please cite this article as: Ilaria Arduino , Zehua Liu , Antti Rahikkala , Patrícia Figueiredo , Alexandra Correia , Annalisa Cutrignelli , Nunzio Denora , Hélder A. Santos , Preparation of Cetyl Palmitate-based PEGylated Solid Lipid Nanoparticles by Microfluidic technique, *Acta Biomaterialia* (2020), doi: https://doi.org/10.1016/j.actbio.2020.12.024

This is a PDF file of an article that has undergone enhancements after acceptance, such as the addition of a cover page and metadata, and formatting for readability, but it is not yet the definitive version of record. This version will undergo additional copyediting, typesetting and review before it is published in its final form, but we are providing this version to give early visibility of the article. Please note that, during the production process, errors may be discovered which could affect the content, and all legal disclaimers that apply to the journal pertain.

© 2020 Published by Elsevier Ltd on behalf of Acta Materialia Inc.

Journal Pre-proof

Preparation of Cetyl Palmitate-based PEGylated Solid Lipid Nanoparticles by Microfluidic technique

Ilaria Arduino[a,b#], Zehua Liu[a#], Antti Rahikkala[a], Patrícia Figueiredo[a], Alexandra Correia[a], Annalisa Cutrignelli[b], Nunzio Denora[a]*, and Hélder A. Santos[b,c]*

[a]Drug Research Program, Division of Pharmaceutical Chemistry and Technology, Faculty of Pharmacy, University of Helsinki, FI-00014 Helsinki, Finland

[b]Department of Pharmacy - Pharmaceutical Sciences, University of Bari "Aldo Moro", Orabona St. 4, 70125, Bari, Italy

[c]Helsinki Institute of Life Science (HiLIFE), University of Helsinki, FI-00014 Helsinki, Finland

***Corrisponding authors**

Prof. Hélder A. Santos (helder.santos@helsinki.fi)

Prof. Nunzio Denora (nunzio.denora@uniba.it; +39 080 544 2767)

# These authors contributed equally

Journal Pre-proof

Graphycal abstract

Keywords: solid lipid nanoparticles, microfluidics, industrial scale up, 3D cell culture, drug delivery

Abstract

In recent years, several studies have shown that the use of solid lipid nanoparticles (SLN) as a colloidal drug delivery system was more advantageous than lipid emulsions, liposomes and polymeric nanoparticles. SLNs have numerous advantages of different nanosystems and rule out many of their drawbacks. Despite the numerous advantages of SLNs, translation from the preclinical formulation to the industrial scale-up is limited. In order to provide a reproducible and reliable method of producing nanoparticles, and thus, obtain an industrial scale-up, several methods of synthesis of nanoparticles by microfluidic have been developed. Microfluidic technique allows a good control and a continuous online synthesis of nanosystems compared to synthesis in bulk, leading to a narrow size distribution, high batch-to-batch reproducibility, as well as to the industrial scale-up feasibility. This work described the optimization process to produce SLNs by microfluidics. The SLNs produced by microfluidics were characterized by complementary optical and morphological techniques and compared with those produced by bulk method. SLNs were loaded with paclitaxel and sorafenib, used as model drugs. The anti-cancer efficiency of the SLNs formulation was estimated with 2D and 3D tumour models of two different cell lines, and the cellular uptake was also established with fluorescence assisted.

Statement of significance:

In this work, we describe the production of a single step continuous production for solid lipid nanoparticles (SLNs) via glass capillary-based microfluidic-chip. Comparing to conventional bulk methods, the current synthesis method showed several advantages, including a continuous production with high yield, good reproducibility and precise control over the properties of SLNs, which are critical pre-conditions for its successful industrialization. The superiority of this microfluidic-based method was confirmed by an overall physicochemical characterization of the produced SLNs. The size of the SLNs was controlled by altering the microfluidic parameters, and SLNs with dimensions ca. 100 nm were feasibly fabricated through parameters optimization. The microfluidics production of SLNs offered a good encapsulation efficiency and drug loading degree for a sustained release manner.

Journal Pre-proof

1. Introduction

The use of nanoparticulate systems for the treatment of diseases is in continuous progress. As a result of their ability to overcome the disadvantages of the drugs currently used, including controlled and extended drug release, increased delivery to tumor site, and reduced systemic toxicity of cytotoxic agents, they are rapidly developing [1] [2]. An ideal candidate for successful clinical translation should have the following features: (1) a simple and biocompatible component; (2) a facile large-scale production method; (3) a satisfied drug loading; and (4) and releasing behaviour and good stability.

Among all nanoparticulate systems, solid lipid nanoparticles (SLNs), have extensively been evaluated as an alternative drug delivery system [3, 4]. The main advantages of SLNs, comparing to conventional nanoparticle-based drug delivery systems, include the inherent biocompatible nature of the starting materials, possibility of obtaining a controlled release of the incorporated drug for several weeks, stability of the nanoparticle system up to 3 years, and more importantly, besides of its hydrophobic backbone, which endow the potent capability for loading hydrophobic drugs, they are also shown to effectively encapsulate hydrophilic drugs [5-7]. Although there are several advantages of SLNs, clinical use is very limited. The main reasons lie in the absence of a method that allows industrial scale-up, batch-to-batch reproducibility and control of the chemical-physical properties of nanomaterials [8].

The production of SLNs by bulk method involves a very long time of preparation, high concentrations of lipids and surfactants, and a large variability between different batches in terms of size and polydispersity of nanoparticles. The great variability of the synthesis conditions and problems associated with limited mixing process represent significant obstacles for SLNs production by conventional bulk method. The difficulties mentioned above became limiting in obtaining nanoparticles with sizes under 200 nm, which are desirable due to their ability to cross spontaneously different biological barriers [9]. Therefore, research in this field is moving in order to identify a new attractive approach capable of finely controlling a mixing process that allows to generate homogeneous nanosystem of elevated quality [10].

Recently, the focus has been on nanosystems synthetic feasibility using microfluidic based method. This new technique ensures SLN production in a reproducible and reliable way [10-20]. Compared to batch-type bulk methods, microfluidics guarantees both a high control of the synthesis conditions and continuous flow production leading to a narrow size distribution (low polydispersity index, PdI), high batch-to-batch reproducibility, as well as to the industrial scale-up feasibility [10]. However, despite the recent works using microfluidics to synthesize liposomes or lipid

nanoparticles [21-26] to our knowledge, there are currently no works concerning the production of SLNs by microfluidic techniques. Polydimethylsiloxane (PDMS) based microfluidics chip is highly sensitive to organic solvents, which is inevitable for SLNs synthesis [10, 27]. In addition, PDMS based microfluidic chips are not resistant to heating, which is usually required for SLNs synthesis. Meanwhile, the hydrophobic nature of PDMS results in the propensity of the lipid aggregation and adsorption on the walls of microfluidic channel. Whereas for glass or silicon based microfluidics chips, despite their chemical inertness to overcome these limitations, the producing methods usually involve harsh and strict conditions, which may further limit the wide application [28]. As an alternative choice, microfluidic chips composed by glass capillary are relative cheap and easy for fabricating, and therefore draw increasing attentions for synthesizing nanoparticles [13, 14, 16-20].

Here, we described a single step continuous production of SLNs via glass capillary based microfluidic chip. Comparing to the conventional bulk methods, which are usually restrained by multiple and complicated preparation steps, low production rate and poor reproducibility, the current synthesis method showed several advantages, including a continuous production with high yield, good reproducibility and precise control over the physical properties of SLNs, which are critical pre-conditions for its successful industrialization. Furthermore, the superiority of this microfluidic-based method, comparing to the conventional bulk method, was confirmed by an overall promoted physicochemical property of the produced SLNs. The size of the produced SLNs was controlled via altering the microfluidic parameters, and herein, SLNs with dimensions around 100 nm were feasibly fabricated through parameters optimization. Sorafenib (SFN) and paclitaxel (PTX) were used as model drugs, in order to test the feasibility of applying SLNs-based nanoformulation in cancer treatment. The microfluidics production of SLNs offered a good encapsulation efficiency and loading degree of the drugs for a sustained release manner. The anti-cancer efficiency of the drug-loaded SLNs formulations was further evaluated with both 2D and 3D tumour models of two different cell lines, and the tumor penetration and cellular uptake was also confirmed with fluorescence assisted imaging.

Journal Pre-proof

2.0. Materials and Methods

2.1. Materials and cell culturing

All chemicals were of the highest purity available and were used as received without further purification or distillation. Distearoyl phosphoethanolamine- polyethylene glycol (DSPE-PEG) and 1,2-Dipalmitoyl-*sn*-glycero-3-phosphoethanolamine-N-[methoxy (poly (ethylene glycol)-2000]c (16:0 PEG-2-PE) was purchased from Avanti Polar Lipids. Cetyl palmitate was purchased from Farmalabor. Paclitaxel (PTX) and sorafenib (SFN) were purchased from Sigma Aldrich. All solvents used were of analytical grade and purchased from Aldrich. 4-[4-(Dihexadecylamino)styryl]-N-methylpyridinium iodide (DiA) was acquired from Thermo Scientific, USA. All aqueous solutions were prepared using water obtained from a Milli- Q gradient A- 10 system (Millipore, 18.2 MΩ·cm, organic carbon content ≥ 4 μg/L. Dulbecco's Modified Eagle's medium (DMEM), heat inactivated fetal bovine serum (FBS), L-glutamine (200 mM), non-essential amino acids (NEAA), penicillin (100 IU/mL), streptomycin (100 mg/mL) and trypsin (2.5%) were acquired from HyClone Waltham, USA. Phosphate buffer saline (10XPBS) and Hank's balanced salt solution (10× HBSS) were purchased from Hyclone. Disposable culture flasks and Petri dishes were from Corning (Glassworks).

2.2. Production of SLNs with bulk method

SLNs were prepared using an oil-in-water homogenization process at high temperature, according to a procedure reported in literature [29]. In particular, 60 mg of cetyl palmitate and 12 mg of 16:0 PEG- 2- PE were co- dissolved in chloroform (1 mL). Afterwards, a homogeneous mixture was obtained by stirring gently and then the chloroform solution was added drop-by-drop into the aqueous solution (ultrapure water, 3 mL), containing Pluronic F68 (2% p/V) at 65 °C and sonicated for 15 min by using an ultrasound probe-tip (0.27 W). The organic phase was rapidly evaporated at 65 °C by means of a rotary evaporator. The aqueous solution was left at room temperature for 2 h to promote the complete evaporation of the organic solvents, and then, it was kept at 4 °C for 15 min to allow the SLNs formation. In order to remove the surfactant and solvent residuals the produced SLNs were carefully purified by using ultrapure water and centrifugal concentrators (Centricon Centriplus YM100) at 800 g for 1 h at 4 °C. The nanoformulation was kept in ultrapure water at 4°C.

2.3. Fabrication of the microfluidic devices

Journal Pre-proof

The microfluidic devices were assembled from borosilicate glass capillaries and glass rods. In this work, two different devices were developed and identified as device 1 (conventional microfluidic chip) and device 2. For device 1, one end of the cylindrical glass capillary (World Precision Instruments, Inc.), with inner and outer diameters of 580 and 1000 μm, respectively, was tapered using a micropipette puller (P-97, Sutter Instrument Co., USA) to a diameter of 20 μm; this diameter was further enlarged to approximately 80 μm by using sand paper (RHYNOWET P-2500, Indasa, USA). This cylindrical tapered capillary was inserted and coaxially aligned into the left end of the cylindrical capillary with inner dimension of 1100 μm (Vitrocom, USA).[30, 31] In the case of device 2, a three-port valve is connected after the device 1. Two miscible (functioning as outer and inner phase for nanoparticle production) liquids were injected separately into the microfluidic device through polyethylene tubes attached to syringes at constant flow rates, and the air was introduced to the solution through the three-port valve to further enhance the mixing efficiency. The flow rate of the different liquids was controlled by pumps (PHD 2000, Harvard Apparatus, USA). A schematic comparison of device 1 and 2 is shown in **Figure S1**.

During the production of SLNs, it was fundamental to keep the temperature above 60 ºC. In this regard, a supporting heating facility was designed and constructed by wrapping the lipid containing syringe with electric wire, which connected with a pressure regulator; the temperature of the electric wire wrapped syringe was controlled by altering the voltage, and the temperature was set to 60 ºC. The microfluidic chip was immersed in water containing heating bath, and the temperature was also maintained at 60 ºC.

2.4. Optimization of SLNs production by microfluidics

The SLNs were prepared by nanoprecipitation in a glass capillary microfluidics device, as mentioned above [14, 16, 17, 19, 32]. In the co-flow geometry, the inner and the outer fluids flow in the same directions. During the nanoprecipitation method, the internal and external solution are pumped into the microfluidic device with a constant flow rate. These solutions are miscible, and two pumps kept the flow rate of the two phases under control and the liquids were transported from the syringes to the capillaries thanks to the use of polyethylene tubes. The lipid matrix was dissolved in an 95% ethanol solution and served as the inner fluid. In addition, an aqueous solution containing stabilizers was selected as the outer continuous fluid. The SLNs synthesis process was optimized through the variation of different parameters, including flow rate, flow speed, type of surfactants (Pluronic F68 (F68), Pluronic F127 (F127), Polyvinyl Alcohol (PVA) at the

concentrations of 2%, 3% and 4% (w/v) and Tween 80 (T80) at the concentrations 1% and 2% (w/v)).

The lipid component of the nanoparticle preparation consisted of cetyl palmitate and DSPE–PEG (3 mg/mL). Different concentrations were tested using cetyl palmitate (10, 50 and 100 mg/mL). Moreover, different inner and outer fluid flow rates were used in order to identify the one that allowed to obtain small SLNs. Both the fluids were injected into microfluidic device from separate inlets at flow rate of 5:10 to 50:100 mL/min. The cooling phase (4°C for 15 min) occurs after the complete evaporation of the organic phase. When SLNs loaded PTX or SFN were produced, the drug was added to the ethanol solution along with the lipids. Specifically, for PTX, concentrations were tested in a range from 0.5 to 1.5 mg/mL and for SFN in a range from 0.2 to 2 mg/mL. The purification of SLNs took place through the dialysis bags, in order to eliminate the surfactant and the unloaded drug. (Spectra/Por 1 Standard RC Dry Dialysis Tubing, 12-14 kDa, Spectrum Labs, USA) for 24 h at 25 °C. All the optimization experiments, i.e., the variation of the different parameters, for the production of the NPs were carried out using the device 1. After identifying the best parameters, device 2 was used in order to compare the results.

2.5. Encapsulation efficiency and drug loading determination

To obtain drug loaded SLNs, PTX and SFN were mixed into the inner fluid. The percentage of encapsulation efficacy (EE%) of PTX and SFN in the SLNs and the drug loading (DL%) was estimated using high-performance liquid chromatography (HPLC, Agilent 1200 Infinity Series). Briefly, 2 mL of DMSO and hexane 1:1 was added to disrupt the SLNs and 20 µL of the resulting transparent solution were injected into HPLC. For PTX a Discovery C18 (150 × 4.6 mm, 5 µm) column and a mobile phase consisting of water and acetonitrile (ACN) (53:47%, v/v), with detection wavelength at 227 nm, flow 1 mL/min, injection volume 20µl, while for SFN a Gemini (3 µm, NX-C18, 110Å) column and a mobile phase consisting of water and 0.1% of trifluoroacetic acid (TFA) and ACN (48:52%, v/v), with detection wavelength at 255 nm, flow 1 ml/min, injection volume 20µl, were used to quantify the targeted drugs. The EE% and DL% were calculated using Eqs. (1) and (2), respectively:

$$Encapsulation\ Efficacy\ (\%) = \frac{Weight\ of\ drug\ in\ SLN}{Weight\ of\ drug\ added\ initially} \times 100 \quad (1)$$

Journal Pre-proof

$$Drug\ Loading\ \ (\%) = \frac{Weight\ of\ drug\ in\ SLN}{Weight\ of\ SLN + Weight\ of\ Drug\ in\ SLN} \times 100$$

(2)

2.6. Characterization of the produced SLNs

The zeta (ζ)-potential and size distribution of the samples were determined using a Zetasizer Nano ZS (Malvern Instruments Ltd., Worcestershire, UK). About 1 mL of a 1:50 dilution of each sample with demineralized water was poured out into a disposable polystyrene cuvette (Sarstedt AG & Co., Germany) and the measurements were carried out at 25 ± 0.1 ºC. The surface potential of the nanoparticles was measured by pipetting 750 µL of each particle suspension into a disposable folder capillary cell (DTS1070, Malvern, UK); the sample was redispersed in MilliQ-water (pH 7.4) before assessing its ζ-potential. The resulting data are indicated as numeric average and standard deviation of the measurements of three different samples, each sample measured three times.

2.7. Transmission electron microscope imaging

The morphology and the size distribution of the SLNs were analysed by a transmission electron microscope (TEM, Jeol JEM-1400, Jeol Ltd., Japan). In order to achieve this, 10 µL of particles suspension were applied to a carbon-coated copper grid (300 mesh; Electron Microscopy Sciences, USA) for 5 min. Then, the samples were negatively stained with uranyl acetate by adding 2 µL of a 2.1% uranyl acetate solution to the grids for ~2 min. The grids were then washed once with 5 µL of Milli-Q water for 5 min to remove the excess of uranyl acetate. Finally, the grids were dried in open air overnight before imaging.

2.8. Stability studies

To evaluate the SLNs short-term stability, the size distribution of SLNs was measured in PBS (pH 7.4), in DMEM supplemented with 10% (v/v) of FBS and in fresh frozen plasma (provided by the Finnish Red Cross). Briefly, 200 µL of SLNs were incubated in 1.5 mL of physiological relevant media at 37 ºC; at defined time points (5, 15, 30, 60, 90, and 120 min), a certain amount of sample was taken, diluted in water in order to analyse the change in size over time. Triplicates of each experiments were performed.

2.9. *In vitro* drug release studies

Release studies of PTX and SFN from the SLNs were performed using Franz cells, [33] [34] in particular the experiments were conducted in the presence and absence of human serum in the donor compartment. Further information can be found in the SI.

2.10. Preparation of the 3D-tumor spheroids

The formation of the 3D-tumor spheroids was achieved through the use of the 3D-bioprinting method [35]. About 1.5 mL of human glioblastoma cell line (U87-MG) (American TypeCulture Collection ATCC, USA) at a density of 400000 cells per well were seeded in 6-well plates and left to incubate overnight in order to allow to attach. Subsequently, 50 µL of Nanoshuttle-PL (Nano3D Biosciences Inc., Germany) was added to the cells, and they were incubated for 8-10 h for magnetization of the cells. Therefore, a double washing of the cells using PBS buffer (pH 7.4) was carried out, and then sowing seeded in ultralow attachment 96-well plates at a density of 5000 cells per well was performed, and this plate was positioned above a 96-well spheroid magnetic drive (Nano3D Biosciences Inc., Germany). The magnetized cells aggregated in the well of the plate, addressed by the magnet, and the spheroids were grown for 2 days [35].

2.11. Cytotoxicity studies

Cytotoxicity experiments were conducted using 2D and 3D-cell cultures of U87-MG cell line and 2D-cell model of human alveolar adenocarcinoma cells line (A549) (American TypeCulture Collection ATCC, USA). For the 2D model, A549 and U87-MG cell lines were seeded in 96-well plates (PerkinElmer Inc., USA) at a density of 15000 cells per well and left attaching overnight. After that, 100 µL of SLNs, PTX-loaded SLNs and SFN-loaded SLNs at different concentrations of the nanoparticles (100, 250, 500, 700, and 1500 µg/mL) were added to each well and the plate were incubated for 24 h at 37 ºC. The concentrations of PTX and SFN tested were 3.3 µM, 4.6 µM, 9.3 µM, 13.0 µM, 27.9 µM and 3.0 µM, 6.1 µM, 12.1 µM, 17.7 µM, 36.5 µM, respectively. Cells incubated with cell media were used as a positive control.

After 24 h of incubation, the plates were kept at room temperature for 30 min and afterward it was washed using 100 µL of HBSS–HEPES buffer. Then, 50 µL of Cell Titer-Glo® (Promega

Corporation, USA) were added to 50 µL of HBSS–HEPES (pH 7.4) in each well. After the plates were shaken for 2 min in an orbital shaker, a stabilisation phase of 30 min was achieved, protecting the plates from light. The luminescence was evaluated using a Varioskan Flash plate reader. Obtained the 3D tumour spheroid prepared with U87 cells, as described above, the spheroids were then retransferred to 96-well plates (PerkinElmer Inc., USA). Then, 50 µL of SLNs, PTX-loaded SLNs and SFN-loaded SLNs suspensions at different concentrations of SLNs and similar concentrations of pure PTX and SFN previously dissolved with 3% (v/v) ethanol were added to each well, and added with 50 µL of NanoLuc luciferase and MT Cell Viability Substrate in complete cell culture medium, up to 24 h at 37 °C [35]. The final concentration of SLNs was 100, 250, 500, 700, and 1500 µg/mL and the free PTX and SFN were the same as described above, and the incubation with cell media was used as positive control. The RealTime-Glo® MT Cell Viability Assay is a nonlytic, homogeneous and bioluminescent way that consents to evaluate the cell viability in real time. After 24 h the luminescence has been determined using a Varioskan Flash plate reader. Triplicates have been performed for each experiment.

2.12. Cell-SLNs interactions using a 3D tumor spheroid model

The cell–SLNs interactions were performed by loading the SLNs with a hydrophobic dye in a mass ratio 100:1 (SLNs:DiA).The interactions between U87-MG cell lines and DiA-loaded SLNs were qualitatively assessed by confocal fluorescence microscopy. As mentioned above, the technique used for the formation of the 3D tumor spheroid was 3D bioprinting. The cell culture medium was removed, and the spheroid was washed with PBS buffer; after this procedure, the spheroids were treated with 100 µL of 100 µg/mL of SLNs' suspension in PBS buffer (pH 7.4) and left at 37 °C for 3 h. A double wash with PBS was carried out below in order to remove the unattached SLNs and the spheroids were then immobilized using 4% paraformaldehyde for 24 h at 37 °C. Afterwards, another double wash (with PBS buffer) was performed, and the nuclei of the cells was observed using 100 µL of DAPI-405 (2.8 µg/mL) and incubated for 6 and 24 h at 37 °C. Finally, the cell spheroids were washed twice with PBS buffer and transferred to a Lab-Tek™ 8-chamber. The interaction of SLNs with the cell was observed with a Leica SP5 inverted confocal microscope (Leica Microsystems, Germany), equipped with a 20× objective.

2.13. Statistical analysis

The experimental data are reported as mean ± SD (standard deviation). Statistical analysis was conducted by Graph Prism version 6.0 (Graphad Sofware Inc., La Jolla, CA, USA). Statistical significance was calculated using a two-way analysis of variance (ANOVA) followed by the Bonferroni post hoc test, set at the probabilities of *** $p<0.001$, **** $p<0.0001$.

3. Results and discussion

3.1.Development and characterization of SLNs

Several papers produced by our research group described the method for the bulk production of SLNs [29, 36]. Although the results are satisfactory, bulk methods provide many steps time-consuming and long times (about 2 days) for obtaining and characterizing the batch. Thus, we hypothesized whether we can apply the microfluidic method to achieve a continuous synthesis of SLNs. However, despite we have previously applied oil-in-water hot homogenization process to prepare the SLNs,[29] herein we choose to apply nanoprecipitation method here for microfluidics based SLNs production. The challenges for producing nano-droplets or emulsions come from the flow dynamics within the microfluidics channel and the mechanisms of droplet production.[16] For nanoemulsion, the free energy of the droplets is higher than the free energy of the separate phases, which means that nanoemulsion is thermodynamically unstable.[37] And the preparation process usually requires a strong energy input. For a typical O/W emulsion with the size 100 nm, input energy intensity is on the order of 10^{8}–10^{10} W kg^{-1}, which set an obstacle for conventional microfluidics production.[16] In the literature it has been widely known that nanoparticles should have size around 100 nm in order to increase the crossing of biological barriers via endocytosis [38-40]. To prove the versatility of the setup, we have synthesized a number of SLNs with different physicochemical properties by varying different parameters. The particle size and PdI as other physicochemical properties of nanoparticles are largely influenced by microfluidic setting and formulation parameters. The use of different surfactants, the variation of surfactant and lipid

concentrations and the flow rate [10], represent the three key parameters that have been varied in order to obtain small SLNs with a low PdI value [19]. The first step to consider for the preparation of SLNs is the temperature. In the bulk method, the SLNs are produced maintaining the temperature around 60 ºC [38, 40]. Therefore, for SLNs produced by microfluidics it was important to achieve a setup that would keep the temperature also around 60 ºC. In this regard, an electronic device was developed, which allowed to maintain the lipids in solution, considering that the melting temperature of cetyl palmitate was 50 ºC. [41] Through the use of a current generator, the syringe, containing the lipids, was wrapped by a metal wire that released heat through the transmission of current. In particular, by means of a voltage of 1.2 mV the temperature of the lipid solution reached 50 ºC. Furthermore, the microfluidic device was immersed in water at 60 ºC and in this way the synthesis of the SLNs occurred at the desired temperature (**Figure 1**). A temperature up to 80 ºC was tested on the current microfluidic chip and no obvious leakage was observed.

The device 1 was used during the optimization process. The inner fluid consisted of an ethanol solution of lipids (cetyl palmitate and DSPE-PEG) and the outer an aqueous solution of surfactant. The first parameter was the flow ratio. Briefly, using a ethanolic solution of cetyl palmitate (50 mg/mL) and DSPE-PEG (3 mg/mL), and a water solution of Pluronic F68 (2% p/V), which correspond to the concentrations used for the synthesis of SLNs in bulk, flow rates ranging from 5.10 to 50:100 (**Table 1**), were varied in order to obtain optimized SLNs. Previous reports suggested that under the relative low flow rate (Reynold number lower than 200), a slight increase of flow rate showed low to no effect on the reducing the size of nanoparticles, as the low flow rate renders to a laminar flow regime within the microfluidic channel [28] [42] [30]. Yet, with the increase of the overall flow speed, the residence time of the mixed solution within the microfluidic channel, which was maintained at 60 ºC, was reduced, and the relatively low mixing time may interfere the size and PdI of the produced NPs. As shown in Table 1, despite the increase of flow rate, the dimensions of the NPs still increased.

Table 1. Values of the size and PdI of SLNs obtained using the microfluidic device 1 at different flow rate ratios.

Formulation	**Inner and outer fluid flow rate**	**d_{mean}(nm)**	**Polydispersity index (PdI)**

	(mL/min)		
1	5:10	178±3	0.23±0.01
2	5:15	181±1	0.23±0.01
3	10:25	250±3	0.30±0.02
4	10:50	254±13	0.33±0.02
5	20:100	226±1	0.21±0.08
6	30:100	252±5	0.23±0.00
7	50:100	274±13	0.26±0.03

As such, we further chose to change the surfactants and their corresponding concentrations. By maintaining the lipid solution at a concentration of 50 mg/mL, 4 surfactants (F68, F127, PVA and T80) and different concentrations (2, 3 and 4%, w/v) were selected to synthesize a series of SLNs with different dimensions and PdI. Firstly, T80 stabilized SLNs aggregated at all concentrations tested (used only at concentrations of 1 and 2% w/v, due to toxicity problems [43]) showed SLNs very large in size (**Table 2**). From the data shown in the **Table 2** we concluded that when using F127, as its concentration increased, the size of the SLNs improved, while with F68 and PVA the trend was the opposite. However, both with F127 and PVA the dimensions of the SLNs were exceeded over 200 nm, while we observed that 2% of F68 (w/v) produced SLNs of dimensions below 200 nm. Specifically, from Table 2 it was evident that the SLNs produced with the F68 at 2% w/v and flow rate of 5:15 were smaller in size with a good PdI value. It has been demonstrated that using surfactants with low molecular weight it is possible to produce nanoparticles with smaller size [6] [44]; this is due to their capability to fill interfacial surface quicker than high molecular surfactants. The current results are in agreement with the former reports, where F68 based SLNs formed smaller particle sizes than PVA and F127 [45] [46].

We assume the reason for this phenomenon we observed from different surfactant maybe due to the physiochemical properties of different surfactants. Previous papers suggested that the growth of SLNs will be arrested when there is sufficient surfactant density on the particle surface to stop further aggregation [16, 47].

Based on that, previous papers purposed that the rate at which the stabilizing reagent can passivate the hydrophobic surface depends on its diffusion coefficient (dominated by the hydrophilic part) and the geometry of the polymer during particle assembly.[48] F127 obtains higher viscosity (3100 *v.s.* 1000, Brookfield, cps; liquids at 25℃, pastes at 60℃, solids at 77℃) but lower hydrophilic block (PEO) wt% (70 *v.s.* 80) [49]. These features from F127 will negatively impact the Flory-Huggins polymer/solvent interaction parameter, further reduce the aqueous diffusion of F127 [50]. The

major difference between Tween 80 and F127/F68, we hypothesize, is mainly due to the hydrophilicity. The hydrophile-lipophile balance (HLB) for T80 is 15, which is far lower than both F68 (>24) and F127 (18-23), which will also majorly affect its diffusion within aqueous solution [50]. In that way, F68 showed the best efficiency in halting the growth of SLNs, and thus conferring a smaller final size.

We simplify the SLNs formation process in the similar way where amphiphilic molecules, such as block copolymers to self-assemble into NPs. In this way, the hydrophobic core material (in the case of SLN, the lipid) is dissolved in a water-miscible solvent. Upon mixing with the aqueous solution containing amphiphilic stabilizing material (in the case of SLN, the surfactants), the supersaturation degree of lipid will boost to form into particles. The supersaturated lipid and hydrophobic block of the surfactant assemble by diffusion-limited aggregation. The high supersaturation eliminates nucleation barriers to assembly, but the growth is arrested when there is sufficient surfactant density on the particle surface to stop further aggregation [15, 38].

Table 2. Values of the size and PdI of SLNs obtained using the microfluidic device 1 at two different flow rate ratios and using different surfactants: Pluronic F68 (F68), Pluronic F127 (F127), Polyvinyl Alcohol (PVA) and Tween 80 (T80).

Journal Pre-proof

Surfactant (%w/v)	Inner and outer fluid flow rate (mL/min)	d_{mean}(nm)	Polydispersity index (PdI)
F68 2%	5:10	221±8	0.10±0.04
F68 2%	5:15	181±5	0.26±0.01
F68 3%	5:10	221±3	0.16±0.02
F68 3%	5:15	253±7	0.18±0.03
F68 4%	5:10	246±3	0.10±0.01
F68 4%	5:15	263±4	0.15±0.02
F127 2%	5:10	553±23	0.35±0.15
F127 2%	5:15	743±105	0.61±0.09
F127 3%	5:10	234±4	0.13±0.01
F127 3%	5:15	363±13	0.34±0.02
F127 4%	5:10	271±5	0.24±0.02
F127 4%	5:15	269±3	0.30±0.07
PVA 2%	5:10	277±2	0.11±0.01
PVA 2%	5:15	224±2	0.10±0.02
PVA 3%	5:10	283±1	0.07±0.01
PVA 3%	5:15	304±1	0.19±0.04
PVA 4%	5:10	286±4	0.23±0.00
PVA 4%	5:15	283±4	0.14±0.04
T80 1%	5:10	1155±50	0.80±0.34
T80 1%	5:15	716±11	0.29±0.20
T80 2%	5:10	221±8	0.59±0.10
T80 2%	5:15	181±5	0.42±0.10

Thus, according to **Table 2**, by employing the surfactant F68 (2%, w/v) and a flow rate of 5:15, the last parameter that was modified was the concentration of the lipid. **Table 3** shows that the lowest concentration yielded SLNs around 180 nm and a PdI value of 0.23. From Table 3, it was possible to conclude that as the lipid concentration decreases, smaller SLNs can be obtained and the dimensional distribution also improved. This effect was most likely related to the increasing viscosity of the inner phase, which led to impeded diffusivity of the ethanolic phase into the aqueous phase, and thus, to a longer mixing time [9, 51]. This data is in agreement with previous report, [52] where a reduced size and narrower PdI can be achieved with microfluidic-synthesized liposome at lower concentration of the lipid [32].

Journal Pre-proof

Table 3. Values of the size and PdI of SLNs obtained using the microfluidic device 1 and different concentrations of cetyl palmitate.

Lipid concentration (mg/mL)	Inner and outer fluid flow rate (mL/min)	d_{mean}(nm)	Polydispersity index (PdI)
10	5:15	178±1	0.23±0.00
50	5:15	183±3	0.20±0.04
100	5:15	670±79	0.08±0.06

Yet, even with the optimized parameters, the size of the produced SLNs was still around 200 nm, which needed further improvements. For the microfluidic device 2, a three-port valve was tandem-connected after the microfluidic device 1 to introduce air in the mixing channel. The introduction of immiscible air will further enhanced the mixing of the solution, and a such improved the physical characterization of produced SLNs [28].

Next, the same parameters were obtained for the SLNs of comparable size and with a significantly lower PdI. However, by using both devices we could not reach dimensions around 100 nm. Thus, the further increase of the flow speed in the microfluidic device 2 generated smaller SLNs, as a result of the improved mixing in the microfluidic device 2 in comparison with the microfluidic device 1. (**Table 4**).

Journal Pre-proof

Table 4. Values of the size and PdI of SLNs obtained using the microfluidic devices 1 and 2 with Pluronic F68 (2 %, p/V) and flow rate 10:50.

Formulation	Microfluidic device	Inner and outer fluid flow rate (mL/min)	d_{mean}(nm)	Polydispersity index (PdI)
1	1	10:50	254±13	0.33±0.02
2	2	10:50	121±1	0.11±0.01

After the optimization of the production process of SLNs by microfluidics, the data obtained were compared with those of SLNs obtained by the bulk method. SLNs prepared using the bulk hot homogenization method [38] had a significantly larger size compared to SLNs prepared using the microfluidics method (**Table 5**). It was possible to observe that the preparation of SLNs by conventional bulk method induces the formation of nanoparticles larger than 200 nm with a high standard deviation resulting in a low reproducibility from batch to batch. However, using the microfluidic technique, the possibility of accurately controlling the mixing of the solutions in the

microfluidic channels ensures controlled and reproducible precipitation [9]. The ζ-potential of SLNs prepared with the two methods were similar (Table 5) with a negative surface charge.

Table 5. Comparison of the size, PdI and ζ-potential values of SLN produced using the microfluidic and bulk methods.

	d_{mean}(nm)	**Polydispersity index (PdI)**	**ζ-potential (mV)**
SLN Bulk method	246±6	0.32±8	-25±0.8
SLN Microfluidics	121±0	0.11±0	-23±0.5

The morphology of PEG-SLNs was then investigated by TEM analysis imaging (**Figure 2**). The TEM images have shown that the particle sizes are comparable to the results obtained with DLS, indicating that the SLNs produced in bulk are larger than those produced in microfluidics (**Figure 2**). Comparing the TEM micrographs, we observed that the SLNs produced by microfluidics are very spherical in shape with respect to the bulk method, and the size around 100 nm (**Figure 2**). No aggregation or agglomeration of the SLNs was detected using both methods. Similar results were obtained for PTX-SLNs and SFN-SLNs (data not shown). These results showed that, SLNs typically manufactured in conventional batch stirred volumes are inadequate, regarding the process controllability and reproducibility of the final product. When working in batch systems, perfect mixing conditions are difficult to achieve. This leads to inhomogeneous distribution of concentration and temperature, which results in broad particle size distributions and substantial batch-to-batch product variability. Variations in particle characteristics are responsible for a wide range of formulation problems, related for instance to bioavailability. On the contrary, microfluidic technique was proved to be able to achieve higher control over the physical properties of the final SLNs, mainly in terms of small mean size and narrow size distribution.

After the promising results, we further synthesized the SLNs loaded with the model drugs, PTX and SFN. In order to achieve the highest encapsulation and drug loading degree possible, different drug concentrations were tested. Specifically, for PTX, the concentrations tested were in a range from 0.5 to 1.5 mg/mL and for SFN in a range from 0.2 to 2 mg/mL. As shown in **Figure 3A,B**, for PTX-SLNs the best concentration achieved was 0.75 mg/mL with EE of 54 % and DL of 1.4 %. While for SFN-SLNs, the best concentration achieved was 0.5 mg/mL with EE of 79% and DL of 1.04 %

(**Figure 3C, D**). From **Figure 2A** we observed an increasing trend from the concentration 0.5 mg/mL to 0.75 mg/mL of PTX and a resulting plateau achieved for the concentration 1 mg/mL and 1.5 mg/mL. We chose to use the 0.75 mg/mL of PTX since this concentration allowed to reach the highest value of DL **(Figure 3B**). On the contrary, the EE and DL of SFN (**Figure 3C**), a decreasing trend was observed for concentrations from 0.5 to 2 mg/mL. As a result of the overall consideration of DL and EE of SFN, we finally chose to use the SFN concentration 0.5 mg/mL for further experiments (**Figure 3D**).

The EE of PTX-SLN and SFN-SLN prepared by bulk homogenization process and microfluidics method were 42±1.5% and 54±2.7% for PTX-SLN, while 65 ± 2.4% and 79 ± 1.2% for SFN-SLN using the two methods, respectively (**Table 6**). For both methods, we observed that the lipid nature of the SLNs permitted the loading with the hydrophobic drug, which is incorporated and stably kept into the lipid core, highlighting that fast mixing by microfluidics improved the EE and DL for both drugs compared to the bulk method.

Journal Pre-proof

Table 6. Comparison of EE and DL of SLNs produced by both microfluidic and bulk methods.

	Encapsulation Efficiency (EE%)	**Drug Loading (DL%)**
PTX-SLN Bulk method	42±1	0.8±0.4
PTX-SLN Microfluidics	54±3	1.4±0.2
SFN-SLN Bulk method	65±2	0.7±0.1
SFN-SLN Microfluidics	79±1	1.0±0.3

The *in vitro* release profiles were conducted in PBS (pH 7.4) with 1% of Tween 80 at 37 ºC by using the Franz-diffusion cell. 1% of Tween 80 was added to support the release of the SFN and PTX, because of their poor solubility in water and maintaining the sink conditions during the release studies. The release studies performed on PTX-SLN and SFN-SLNs produced by the bulk method showed no release of PTX and SFN in 120 h, which was further confirmed by a mass balance study (data not shown), thus highlighting the consistent stability of the SLNs. However, in

order to demonstrate the effective release of PTX and SFN from SLNs, we also performed the experiments with human serum in the donor compartment. From the release profiles, we observed that in the presence of human serum, the percentage of the released drug reached 100% (**Figure 4**).

SLNs presented an optimal colloidal stability without proof of aggregation, as revealed by the stability studies realized over 2 h at 37 ºC in PBS (**Figure 5A**), cell medium (**Figure 5B**) and human plasma (**Figure 5C**). The current stability results further confirmed the satisfied serum stability of the prepared SLNs formulation, which is the critical pre-condition for its further success clinical translation.

3.2.Cytotoxicity studies

Next, we further conducted the following *in vitro* experiments to test the microfluidic-produced SLN formulations for anti-cancer applications. 2D-cell models and 3D-tumor spheroids were used to evaluate the cytotoxic effect of PTX-SLNs and SFN-SLNs in human alveolar adenocarcinoma (A549) and human glioblastoma cell lines (U87-MG) and were compared to that of the free administered drugs. First, we confirmed the blank SLNs as vehicle showed a very good cytocompatibility after 24 h incubation with A549 and U87-MG cells (**Figure 6A,B**), with over 80% cell viability at highest concentration tested (1500 µg/mL). In U87-MG cells, SFN-SLNs at concentrations of 250, 500 and 700 µg/mL (SFN concentrations of 6.1 µM, 12.1 µM and 17.7 µM, respectively) showed a reduction in cell viability of 32%, 39% and 52%, respectively, after 24 h incubation (**Figure 6A**). Instead, for free SFN at the same concentrations, the cell viability reduction was 8%, 34% and 50%, respectively. At the lowest concentration the data was statistically significant ($p<0.0001$). Moreover, concentrations of PTX-SLNs at the same SLNs concentrations (PTX concentrations of 3.3 µM, 4.6 µM, and 9.3 µM) showed a cell viability reduction of 35%, 57% and 52%, respectively (**Figure 6A**), and the cell viability reduction for free PTX at the same concentrations were 4%, 13% and 15%, respectively. The data were statistically significant at all concentrations ($p < 0.0001$).

The cancer cell viability inhibition provided by the SFN-SLNs and PTX-SLNs were relatively higher than the free drug counterparts, which may due to the enhanced drug solubility, controlled release of SFN and PTX from the SLNs, as well as the increased cellular internalization due to the

nanoformulation of the drugs [53] [54]. A similar tendency was observed for A549 cells; at the SLNs concentration of 500 and 700 µg/mL, SFN-SLNs (SFN concentrations of 12.1 µM and 17.7 µM) reduced the cell viability to 62% and 46%, respectively (Figure 6B). Instead, for free SFN at the same concentrations, the cell viability reduction was 68% and 79%, respectively. In the case of PTX-SLNs, for the concentrations of 700 and 1500 µg/mL (PTX concentrations of 13.0 µM and 27.9 µM), induced a cell viability reduction to 52% and 59%, respectively (Figure 6B). The free PTX at the same concentrations reduced the cell viability to 51% and 47%. The results for PTX-SLNs were statistically significant ($p<0.0001$). For this cell line, PTX-SLN showed a greater cytotoxic effect compared to the free drug and to SFN-SLNs, which only at the highest drug concentration showed slightly a greater effect than the free drug. The free drug confirmed its anticancer activity both for SFN (at all concentrations) and for PTX (at concentrations of 13.0 µM and 27.9 µM). The different properties of the SLNs including size, shape, composition and surface change are important for the cell–NP interactions, and therefore, for the cytocompatibility of nanosystems [55, 56]. Cetyl palmitate and DSPE-PEG were designated as main component of the SLNs, and the results assured their suitability to produce highly biocompatible NPs with excellent colloidal stability, and further facilitate the potent clinical translation.

Overall, these results indicated good cytocompatibility of the plain SLNs. Contrariwise, the PTX-SLNs and SFN-SLNs showed an overall better anti-proliferative effect against tumor cells compared to the free drugs, indicating that the drug penetration into the cells was probably improved by the encapsulation of the drugs inside the SLN matrix and the endocytosis of SLNs [57]. In the literature, various studies are documented which highlight how the use of SLNs represents a novel and exciting approach to enhance drug delivery into the cells [38, 39, 58]. Moreover, as widely reported, nanoparticles size control is one of the most important parameters to promote cell internalization [59]. Generally, it has been observed a decreasing of nanoparticle uptake efficiency according to larger particle size, likely due to the need for more complex rearrangement by membranes for the internalization of larger structures [60]. Microfluidics-assisted nanoparticle production is known to have the capability to enhance the physical properties of the nanoparticles, including narrower size distribution and high batch-to-batch reproducibility [9, 10, 14, 19, 27]. In this work, using the microfluidics method, we produced SLNs with the size around 100 nm and relatively low PdI, which is the fundamental requirement for the enhanced nanoparticle cell internalization.

However, conventional 2D cell cultures are not able to imitate the complex and heterogeneous nature of clinical solid tumours. Thus, we next evaluated the SLNs cytotoxicity in 3D-tuomor cell spheroids, which are able to mimic a specific organization and architecture of solid tumors,

rendering the potential of 3D cellular spheroids to be used as *in vitro* models for screening new anticancer treatment regime. [35, 61] To further access the solid tumour penetration and anticancer efficiency of both SFN-SLNs and PTX-SLNs, the 3D-spheroid model was equipped using the bio-printing method [35]. Based on the results from 2D model, only U87-MG cell were selected for constructing the 3D-shperoid model for further evaluation. After 24 h incubation, SFN-SLNs at concentrations of 250, 500, 700 and 1500 µg/mL (SFN concentrations of 6.1 µM, 12.1 µM, 17.7 µM and 36.5 µM, respectively), showing a cell viability reduction to 42%, 44%, 50% and 41%, respectively (**Figure 6C**). Instead, for free SFN at the same concentrations, the cell viability was reduced to 9%, 48%, 45% and 41%, respectively. In the case of PTX-SLNs at the concentrations of 700 and 1500 µg/mL (PTX concentrations of 13.0 µM and 27.9 µM) led to a decrease in cell viability to 35% and 25%, respectively (**Figure 6C**). Compared to the 2D cell model, the 3D-spheroid model showed a higher cell viability at the same concentration tested in terms of both SLNs and drugs. This may be due to the minor cell NP interactions of the cells in the 3D culturing models compared to the 2D model, inducing a decrease of the anti-proliferative effect of the cytotoxicity compounds that perform more potently on the proliferating cells [62] [35].

These data revealed that PTX-SLNs and SFN-SLNs are an ideal drug delivery system for the study anti-cancer drugs. In U-87 cells the SLNs showed a higher anti-cancer activity compared to the free drugs (**Figure 6A**). The data demonstrated the great SLN capability to penetrate cancer cell in comparison with free drug. The nanoparticles show the ability to avoid drug efflux pumps located in human cancer cells, consequently raising intracellular drug concentration [63] [64]. Also, in the 3D-tumor spheroids model the SLNs showed a very good cytocompatibility, with cell viability higher than 80% for the concentrations tested (**Figure 6C**).

Journal Pre-proof

3.3.Cell–SLN interaction studies

Conventionally, to evaluate cellular uptake of nanoparticles it is used a 2D model in a flat cell culturing surface. However, this exemplified model is not able to mimic the 3D structure and morphology of physiological tissue; for this reason, the cell–cell interactions do not mimic the *in vivo* situation, inducing errors in the interpretation of cell uptake and overestimating the effectiveness of nanoparticles compared to the 3D model [65]. Here, we evaluated qualitatively the cellular interaction of SLNs with U87-MG cells by confocal fluorescence microscopy. The SLNs were loaded with a highly stable fluorescent dye (DiA, 4-[4-(dihexadecylamino)-styryl]-N-methylpyridinium iodide) and incubated with U87-MG cell for 6 h and 24 h. The confocal

microscopy images of the 3D-tumor spheroids showed already interaction of SLNs with the cells after 6 h incubation at the concentration of 1000 µg/mL of SLNs (**Figure 7**). After 24 h incubation, it was possible to observe the interaction of SLNs with the cells even at the lowest concentration; with interaction we mean an exclusively qualitative evaluation of the permeation of the spheroid by the SLNs (**Figure 7**). As reported in the literature, SLNs of cetyl palmitate were exploited for internalization studies, and the results confirmed that the synthesized NPs with an average diameter of 200 nm and a surface charge of −20 mV were internalized by gliomas in a higher amount than macrophages [66].

Moreover, the evaluation of the cellular uptake mechanism was performed, involving SLNs loaded with rhodamine 123, and it was noticed that the nanoparticles were internalized by clathrin-dependent endocytic pathway [66].

Journal Pre-proof

4. Conclusions

Here, for the first time, we described the production of SLNs using microfluidics followed with systematic optimization process. We showed how the variation of different production parameters influence the size of the SLNs by microfluidics. The produced SLNs by microfluidics were compared with the bulk method in terms of size, PdI and EE, and we concluded that SLNs produced by microfluidics were superior in terms of morphology, size, PdI and simplicity comparing to its bulk counterparts. The DLS size analysis indicated that SLNs samples showed homogenous and monomodal size distribution with an average hydrodynamic diameter around 100 nm, according to TEM images. PTX and SFN, used as model drugs, were successfully encapsulated in the SLNs, and the anti-cancer application of the produced SLNs was further demonstrated *in vitro* in A549 and U87-MG cancer cells. The cytotoxic effect on 2D and 3D cell models of the drugs was greater when they were loaded in SLNs compared to the free drugs. The production of SLNs using microfluidics presented here open a new avenue for the future standardization and scale-up of the production of such nanosystems for biomedical applications.

Acknowledgements

Nunzio Denora acknowledges the University of Bari “Aldo Moro” (Italy) and Angelini A.C.R.A.F. R&D for their financial and technical support. H. A. Santos acknowledges the financial support

from the HiLIFE Research Funds, the Sigrid Jusélius Foundation and the Academy of Finland (grant no. 317042).

References

[1] N. Depalo, R.M. Iacobazzi, G. Valente, I. Arduino, S. Villa, F. Canepa, V. Laquintana, E. Fanizza, M. Striccoli, A. Cutrignelli, A. Lopedota, L. Porcelli, A. Azzariti, M. Franco, M.L. Curri, N. Denora, Sorafenib delivery nanoplatform based on superparamagnetic iron oxide nanoparticles magnetically targets hepatocellular carcinoma, Nano Research 10(7) (2017) 2431-2448.
[2] A. Lopalco, A. Cutrignelli, N. Denora, A. Lopedota, M. Franco, V. Laquintana, Transferrin Functionalized Liposomes Loading Dopamine HCl: Development and Permeability Studies across an In Vitro Model of Human Blood-Brain Barrier, Nanomaterials (Basel) 8(3) (2018).
[3] N.J. Abbott, L. Ronnback, E. Hansson, Astrocyte-endothelial interactions at the blood-brain barrier, Nature reviews. Neuroscience 7(1) (2006) 41-53.
[4] I.P. Kaur, r. bhandari, S. Bhandari, V. Kakkar, Potential of solid lipid nanoparticles in brain targeting, Journal of controlled release : official journal of the Controlled Release Society 127 (2008) 97-109.
[5] I.P. Kaur, R. Bhandari, S. Bhandari, V. Kakkar, Potential of solid lipid nanoparticles in brain targeting, J Control Release 127(2) (2008) 97-109.
[6] C. Tapeinos, M. Battaglini, G. Ciofani, Advances in the design of solid lipid nanoparticles and nanostructured lipid carriers for targeting brain diseases, J Control Release 264 (2017) 306-332.
[7] B. Rohit, K.I. Pal, A method to prepare solid lipid nanoparticles with improved entrapment efficiency of hydrophilic drugs, Current Nanoscience 9(2) (2013) 211-220.
[8] S. Svenson, Clinical translation of nanomedicines, Current Opinion in Solid State and Materials Science 16(6) (2012) 287-294.
[9] N. Lababidi, V. Sigal, A. Koenneke, K. Schwarzkopf, A. Manz, M. Schneider, Microfluidics as tool to prepare size-tunable PLGA nanoparticles with high curcumin encapsulation for efficient mucus penetration, Beilstein Journal of Nanotechnology 10 (2019) 2280-2293.
[10] D. Liu, S. Cito, Y. Zhang, C.-F. Wang, T.M. Sikanen, H.A. Santos, A Versatile and Robust Microfluidic Platform Toward High Throughput Synthesis of Homogeneous Nanoparticles with Tunable Properties, Advanced Materials 27(14) (2015) 2298-2304.
[11] F. Fontana, M.P.A. Ferreira, A. Correia, J. Hirvonen, H. Santos, Microfluidics as a Cutting-Edge Technique for Drug Delivery Applications, Journal of Drug Delivery Science and Technology 34 (2016) 76–87.
[12] A. Gdowski, K. Johnson, S. Shah, I. Gryczynski, J. Vishwanatha, A. Ranjan, Optimization and scale up of microfluidic nanolipomer production method for preclinical and potential clinical trials, Journal of Nanobiotechnology 16 (2018).
[13] L.-H. Hung, A. Lee, Microfluidic devices for the synthesis of nanoparticles and biomaterials, Journal of Medical and Biological Engineering 27 (2006) 1-6.
[14] D. Liu, H. Zhang, F. Fontana, J. Hirvonen, H. Santos, Microfluidic-Assisted Fabrication of Carriers for Controlled Drug Delivery, Lab on a Chip 17 (2017) 1856-1883.
[15] D. Liu, H. Zhang, F. Fontana, J.T. Hirvonen, H.A. Santos, Current developments and applications of microfluidic technology toward clinical translation of nanomedicines, Advanced Drug Delivery Reviews 128 (2018) 54-83.
[16] Z. Liu, F. Fontana, A. Python, J.T. Hirvonen, H.A. Santos, Microfluidics for Production of Particles: Mechanism, Methodology, and Applications, Small 16(9) (2020) 1904673.
[17] J.P. Martins, G. Torrieri, H. Santos, The importance of microfluidics for the preparation of nanoparticles as advanced drug delivery systems, Expert Opinion on Drug Delivery 15 (2018) 469-479.

[18] H. Santos, Opinion Paper: Microfluidics Technique to Revolutionize the Drug Delivery Field: Current Developments and Applications, Current Drug Delivery 12 (2015) 642-644.
[19] N. Tahir, A. Madni, W. Li, A. Correia, M.M. Khan, M.A. Rahim, H.A. Santos, Microfluidic fabrication and characterization of Sorafenib-loaded lipid-polymer hybrid nanoparticles for controlled drug delivery, International Journal of Pharmaceutics 581 (2020) 119275.
[20] S. Wang, S. Wannasarit, P. Figueiredo, J. Li, A. Correia, B. Xia, R. Wiwattanapatapee, J. Hirvonen, D. Liu, W. Li, H.A. Santos, Superfast and controllable microfluidic inking of anti-inflammatory melanin-like nanoparticles inspired by cephalopods, Materials Horizons 7(6) (2020) 1573-1580.
[21] N. Forbes, M.T. Hussain, M.L. Briuglia, D.P. Edwards, J.H.t. Horst, N. Szita, Y. Perrie, Rapid and scale-independent microfluidic manufacture of liposomes entrapping protein incorporating in-line purification and at-line size monitoring, International Journal of Pharmaceutics 556 (2019) 68-81.
[22] N. Dimov, E. Kastner, M. Hussain, Y. Perrie, N. Szita, Formation and purification of tailored liposomes for drug delivery using a module-based micro continuous-flow system, Scientific Reports 7(1) (2017) 12045.
[23] M. Guimarães Sá Correia, M.L. Briuglia, F. Niosi, D.A. Lamprou, Microfluidic manufacturing of phospholipid nanoparticles: Stability, encapsulation efficacy, and drug release, International journal of pharmaceutics 516(1-2) (2017) 91-99.
[24] S. Joshi, M.T. Hussain, C.B. Roces, G. Anderluzzi, E. Kastner, S. Salmaso, D.J. Kirby, Y. Perrie, Microfluidics based manufacture of liposomes simultaneously entrapping hydrophilic and lipophilic drugs, International journal of pharmaceutics 514(1) (2016) 160-168.
[25] C. Liu, W. Zhang, Y. Li, J. Chang, F. Tian, F. Zhao, Y. Ma, J. Sun, Microfluidic Sonication To Assemble Exosome Membrane-Coated Nanoparticles for Immune Evasion-Mediated Targeting, Nano Letters 19(11) (2019) 7836-7844.
[26] L. Zhang, Q. Chen, Y. Ma, J. Sun, Microfluidic Methods for Fabrication and Engineering of Nanoparticle Drug Delivery Systems, ACS Applied Bio Materials 3(1) (2020) 107-120.
[27] P.M. Valencia, E.M. Pridgen, M. Rhee, R. Langer, O.C. Farokhzad, R. Karnik, Microfluidic Platform for Combinatorial Synthesis and Optimization of Targeted Nanoparticles for Cancer Therapy, ACS Nano 7(12) (2013) 10671-10680.
[28] L. Zehua, F. Flavia, P. Andre, T.H. Jouni, A.S. Hélder, Microfluidics for Production of Particles: Mechanism, Methodology, and Applications, Small 16(9) (2020).
[29] I. Arduino, N. Depalo, F. Re, R. Dal Magro, A. Panniello, N. Margiotta, E. Fanizza, A. Lopalco, V. Laquintana, A. Cutrignelli, A.A. Lopedota, M. Franco, N. Denora, PEGylated solid lipid nanoparticles for brain delivery of lipophilic kiteplatin Pt(IV) prodrugs: An in vitro study, International Journal of Pharmaceutics 583 (2020) 119351.
[30] Z. Liu, Y. Li, W. Li, W. Lian, M. Kemell, S. Hietala, P. Figueiredo, L. Li, E. Mäkilä, M. Ma, J. Salonen, J.T. Hirvonen, D. Liu, H. Zhang, X. Deng, H.A. Santos, Close-loop dynamic nanohybrids on collagen-ark with in situ gelling transformation capability for biomimetic stage-specific diabetic wound healing, Materials Horizons 6(2) (2019) 385-393.
[31] Z. Liu, Y. Li, W. Li, C. Xiao, D. Liu, C. Dong, M. Zhang, E. Mäkilä, M. Kemell, J. Salonen, J.T. Hirvonen, H. Zhang, D. Zhou, X. Deng, H.A. Santos, Multifunctional Nanohybrid Based on Porous Silicon Nanoparticles, Gold Nanoparticles, and Acetalated Dextran for Liver Regeneration and Acute Liver Failure Theranostics, Advanced Materials 30(24) (2018) 1703393.
[32] C. Costa, Z. Liu, J.P. Martins, A. Correia, P. Figueiredo, A. Rahikkala, W. Li, J. Seitsonen, J. Ruokolainen, S.-P. Hirvonen, A. Aguiar-Ricardo, M.L. Corvo, H.A. Santos, All-in-one microfluidic assembly of insulin-loaded pH-responsive nano-in-microparticles for oral insulin delivery, Biomaterials Science 8(12) (2020) 3270-3277.
[33] A. Lopedota, A. Cutrignelli, V. Laquintana, N. Denora, R.M. Iacobazzi, M. Perrone, E. Fanizza, M. Mastrodonato, D. Mentino, A. Lopalco, N. Depalo, M. Franco, Spray Dried Chitosan

Microparticles for Intravesical Delivery of Celecoxib: Preparation and Characterization, Pharmaceutical Research 33(9) (2016) 2195-2208.
[34] A. Lopedota, N. Denora, V. Laquintana, A. Cutrignelli, A. Lopalco, D. Tricarico, F. Maqoud, A. Curci, M. Mastrodonato, F. la Forgia, S. Fontana, M. Franco, Alginate-Based Hydrogel Containing Minoxidil/Hydroxypropyl-β-Cyclodextrin Inclusion Complex for Topical Alopecia Treatment, J Pharm Sci 107(4) (2018) 1046-1054.
[35] P. Figueiredo, M. Sipponen, K. Lintinen, A. Correia, A. Kiriazis, J. Yli-Kauhaluoma, M. Österberg, A. George, J. Hirvonen, M. Kostiainen, H. Santos, Preparation and Characterization of Dentin Phosphophoryn- Derived Peptide- Functionalized Lignin Nanoparticles for Enhanced Cellular Uptake, Small 15 (2019) 1901427.
[36] I. Arduino, R.M. Iacobazzi, C. Riganti, A.A. Lopedota, M.G. Perrone, A. Lopalco, A. Cutrignelli, M. Cantore, V. Laquintana, M. Franco, N.A. Colabufo, G. Luurtsema, M. Contino, N. Denora, Induced expression of P-gp and BCRP transporters on brain endothelial cells using transferrin functionalized nanostructured lipid carriers: A first step of a potential strategy for the treatment of Alzheimer's disease, Int J Pharm 591 (2020) 120011.
[37] A. Gupta, H.B. Eral, T.A. Hatton, P.S. Doyle, Controlling and predicting droplet size of nanoemulsions: scaling relations with experimental validation, Soft Matter 12(5) (2016) 1452-1458.
[38] I. Arduino, N. Depalo, F. Re, R. Dal Magro, A. Panniello, N. Margiotta, E. Fanizza, A. Lopalco, V. Laquintana, A. Cutrignelli, A. Assunta Lopedota, M. Franco, N. Denora, PEGylated Solid Lipid Nanoparticles for Brain Delivery of Lipophilic Kiteplatin Pt(IV) Prodrugs: an In Vitro Study, Int J Pharm (2020) 119351.
[39] D. Chirio, M. Gallarate, E. Peira, L. Battaglia, E. Muntoni, C. Riganti, E. Biasibetti, M.T. Capucchio, A. Valazza, P. Panciani, M. Lanotte, L. Annovazzi, V. Caldera, M. Mellai, G. Filice, S. Corona, D. Schiffer, Positive-charged solid lipid nanoparticles as paclitaxel drug delivery system in glioblastoma treatment, Eur J Pharm Biopharm 88(3) (2014) 746-58.
[40] R.H. Muller, K. Mader, S. Gohla, Solid lipid nanoparticles (SLN) for controlled drug delivery - a review of the state of the art, Eur J Pharm Biopharm 50(1) (2000) 161-77.
[41] U. Ruktanonchai, S. Limpakdee, S. Smith, U. Hanusch, N. Bunyapraphatsara, V. Junyaprasert, The effect of cetyl palmitate crystallinity on physical properties of gamma-oryzanol encapsulated in solid lipid nanoparticles, Nanotechnology 19 (2008) 095701.
[42] Z. Liu, Y. Li, W. Li, C. Xiao, D. Liu, C. Dong, M. Zhang, E. Mäkilä, M. Kemell, J. Salonen, J.T. Hirvonen, H. Zhang, D. Zhou, X. Deng, H.A. Santos, Multifunctional Nanohybrid Based on Porous Silicon Nanoparticles, Gold Nanoparticles, and Acetalated Dextran for Liver Regeneration and Acute Liver Failure Theranostics, Adv Mater 30(24) (2018) e1703393.
[43] S. Gupta, R. Kesarla, N. Chotai, A. Misra, A. Omri, Systematic Approach for the Formulation and Optimization of Solid Lipid Nanoparticles of Efavirenz by High Pressure Homogenization Using Design of Experiments for Brain Targeting and Enhanced Bioavailability, Biomed Res Int 2017 (2017) 5984014.
[44] J. Pardeike, S. Weber, T. Haber, J. Wagner, H.P. Zarfl, H. Plank, A. Zimmer, Development of an itraconazole-loaded nanostructured lipid carrier (NLC) formulation for pulmonary application, Int J Pharm 419(1-2) (2011) 329-38.
[45] H. Ebrahimi, Y. Javadzadeh, M. Hamidi, M. Barzegar-Jalali, Repaglinide-loaded solid lipid nanoparticles: Effect of using different surfactants/stabilizers on physicochemical properties of nanoparticles, DARU Journal of Pharmaceutical Sciences 23 (2015).
[46] A. Kovacevic, S. Savic, G. Vuleta, R.H. Müller, C.M. Keck, Polyhydroxy surfactants for the formulation of lipid nanoparticles (SLN and NLC): Effects on size, physical stability and particle matrix structure, International Journal of Pharmaceutics 406(1) (2011) 163-172.
[47] P.M. Valencia, O.C. Farokhzad, R. Karnik, R. Langer, Microfluidic technologies for accelerating the clinical translation of nanoparticles, Nat Nanotechnol 7(10) (2012) 623-9.

Journal Pre-proof

[48] R.F. Pagels, J. Edelstein, C. Tang, R.K. Prud'homme, Controlling and Predicting Nanoparticle Formation by Block Copolymer Directed Rapid Precipitations, Nano Letters 18(2) (2018) 1139-1144.
[49] P. Alexandridis, T. Alan Hatton, Poly(ethylene oxide)□poly(propylene oxide)□poly(ethylene oxide) block copolymer surfactants in aqueous solutions and at interfaces: thermodynamics, structure, dynamics, and modeling, Colloids and Surfaces A: Physicochemical and Engineering Aspects 96(1) (1995) 1-46.
[50] J. Zielinski, J. Duda, Predicting Polymer/Solvent Diffusion Coefficients Using Free-Volume Theory, AIChE Journal 38 (1992) 405-415.
[51] S.M. D'Addio, R.K. Prud'homme, Controlling drug nanoparticle formation by rapid precipitation, Advanced Drug Delivery Reviews 63(6) (2011) 417-426.
[52] M. Maeki, Y. Fujishima, Y. Sato, T. Yasui, N. Kaji, A. Ishida, H. Tani, Y. Baba, H. Harashima, M. Tokeshi, Understanding the formation mechanism of lipid nanoparticles in microfluidic devices with chaotic micromixers, PLoS One 12(11) (2017) e0187962.
[53] A. Janoniene, Z. Liu, L. Baranauskiene, E. Mäkilä, M. Ma, J. Salonen, J. Hirvonen, H. Zhang, V. Petrikaite, H.A. Santos, A Versatile Carbonic Anhydrase IX Targeting Ligand-Functionalized Porous Silicon Nanoplatform for Dual Hypoxia Cancer Therapy and Imaging, ACS Applied Materials & Interfaces 9(16) (2017) 13976-13987.
[54] Z. Liu, V. Balasubramanian, C. Bhat, M. Vahermo, E. Mäkilä, M. Kemell, F. Fontana, A. Janoniene, V. Petrikaite, J. Salonen, J. Yli-Kauhaluoma, J. Hirvonen, H. Zhang, H.A. Santos, Quercetin-Based Modified Porous Silicon Nanoparticles for Enhanced Inhibition of Doxorubicin-Resistant Cancer Cells, Adv Healthc Mater 6(3) (2017).
[55] P. Foroozandeh, A. Abdul Aziz, Insight into Cellular Uptake and Intracellular Trafficking of Nanoparticles, Nanoscale Research Letters 13 (2018).
[56] M. Zhu, G. Nie, H. Meng, T. Xia, A. Nel, Y. Zhao, Physicochemical properties determine nanomaterial cellular uptake, transport, and fate, Accounts of chemical research 46(3) (2013) 622-631.
[57] H. Yuan, J. Miao, Y.-Z. Du, J. You, F.-Q. Hu, S. Zeng, Cellular uptake of solid lipid nanoparticles and cytotoxicity of encapsulated paclitaxel in A549 cancer cells, International Journal of Pharmaceutics 348(1) (2008) 137-145.
[58] M.M. Patel, B.M. Patel, Crossing the Blood-Brain Barrier: Recent Advances in Drug Delivery to the Brain, CNS Drugs 31(2) (2017) 109-133.
[59] A.M. Bannunah, D. Vllasaliu, J. Lord, S. Stolnik, Mechanisms of Nanoparticle Internalization and Transport Across an Intestinal Epithelial Cell Model: Effect of Size and Surface Charge, Molecular Pharmaceutics 11(12) (2014) 4363-4373.
[60] V. Francia, D. Montizaan, A. Salvati, Interactions at the cell membrane and pathways of internalization of nano-sized materials for nanomedicine, Beilstein Journal of Nanotechnology 11 (2020) 338-353.
[61] E. Fröhlich, Comparison of conventional and advanced in vitro models in the toxicity testing of nanoparticles, Artificial cells, nanomedicine, and biotechnology 46(sup2) (2018) 1091-1107.
[62] E. Froehlich, Comparison of conventional and advanced in vitro models in the toxicity testing of nanoparticles, Artificial Cells, Nanomedicine, and Biotechnology 46 (2018) 1-17.
[63] A. Grillone, M. Battaglini, S. Moscato, L. Mattii, C. De Julián Fernández, A. Scarpellini, M. Giorgi, E. Sinibaldi, G. Ciofani, Nutlin-loaded magnetic solid lipid nanoparticles for targeted glioblastoma treatment, Nanomedicine 14 (2019) 727-752.
[64] B. Li, H. Xu, Z. Li, M. Yao, M. Xie, H. Shen, S. Shen, X. Wang, Y. Jin, Bypassing multidrug resistance in human breast cancer cells with lipid/polymer particle assemblies, International journal of nanomedicine 7 (2012) 187-197.
[65] S. Behzadi, N. Vatan, K. Lema, D. Nwaobasi, I. Zenkov, P. Abadi, D.A. Khan, C. Corbo, H. Aghaverdi, O. Farokhzad, M. Mahmoudi, Flat Cell Culturing Surface May Cause Misinterpretation of Cellular Uptake of Nanoparticles, Advanced Biosystems 2 (2018) 1800046.

Journal Pre-proof

[66] S. Martins, S. Costa-Lima, T. Carneiro, A. Cordeiro-da-Silva, E.B. Souto, D.C. Ferreira, Solid lipid nanoparticles as intracellular drug transporters: an investigation of the uptake mechanism and pathway, Int J Pharm 430(1-2) (2012) 216-27.

mmc1.docx

Declaration of interests

☒ The authors declare that they have no known competing financial interests or personal relationships that could have appeared to influence the work reported in this paper.

Figure 1. Schematic representation of setup producing SLNs through microfluidics.

Figure 2. Representative TEM micrographs obtained with staining for SLNs. (A) TEM micrographs of SLNs obtained with bulk method. (B) TEM micrographs of SLNs obtained with the microfluidic method.

Figure 3. Drug encapsulation efficiency (EE) and drug loading (DL) of PTX (A and B, respectively) and SFN (C and D, respectively) using different concentrations of drug. Mean ± SD are reported, n=3.

Figure 4. *In vitro* release profiles of PTX (A) and SFN (B) from SLNs in PBS at 37 ºC. SLNs were diluted with water or human serum in the donor compartment. Mean ± SD are reported, n=3.

Figure 5. Stability studies of SLNs: hydrodynamic diameter and PdI index in (A) PBS (pH 7.4), (B) cell medium and (C) human plasma at 37°C after 2 h. Mean ± SD are reported, n=3.

Figure 6. Cell viability studies of SLNs, SLN-PTX, SLN-SFN, free PTX and SFN using a 2D cell model of U87-MG (A) and A549 (B) cell lines, and (C) 3D-spheroid cell model of U87-MG cell line after incubation for 24 h at 37 ºC, and determined by the CellTiter-Glo® luminescence assay. All data sets were compared to the positive control (cell medium). Each drug was tested in triplicate, and the experiments were repeated three times. Statistical significance was calculated using a two-way analysis of variance (ANOVA) followed by the Bonferroni post hoc test, set at the probabilities of *** $p<0.001$, **** $p<0.0001$.

Figure 7. *In vitro* cellular interaction studies using a 3D-spheroid tumor model. Confocal fluorescence microscope images of U87-MG cells after incubation with 500 and 1000 µg/mL of DiA-SLNs for 6 h and 24 h at 37 °C. DAPI (blue) and DiA (green) were used to stain the nucleus and the SLNs, respectively. Scale bars are 250 µm.

Journal Pre-proof